Open Access

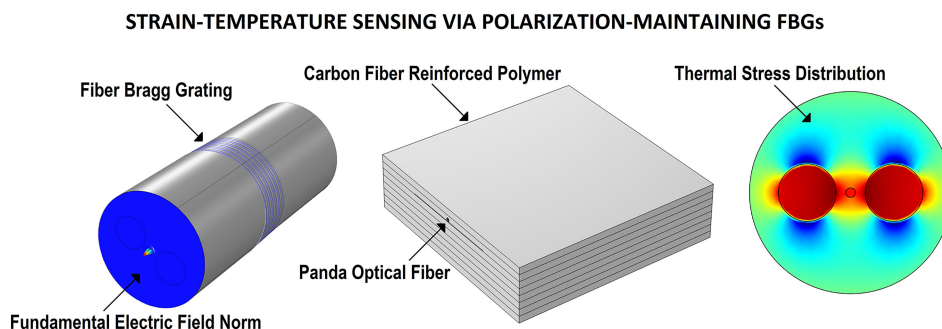# Design of Polarization-Maintaining FBGs Using Polyimide Films to Improve Strain-Temperature Sensing in CFRP Laminates

Andrea Annunziato
Francesco Anelli
James Gates
Christopher Holmes
Francesco Prudenzano, *Member, IEEE*

STRAIN-TEMPERATURE SENSING VIA POLARIZATION-MAINTAINING FBGs

Fiber Bragg Grating
Carbon Fiber Reinforced Polymer
Thermal Stress Distribution
Fundamental Electric Field Norm
Panda Optical Fiber

IEEE

Design of Polarization-Maintaining FBGs Using Polyimide Films to Improve Strain-Temperature Sensing in CFRP Laminates

Andrea Annunziato,[1] **Francesco Anelli** [ORCID]**,**[1] **James Gates** [ORCID]**,**[2] **Christopher Holmes,**[2] **and Francesco Prudenzano** [ORCID]**,**[1] *Member, IEEE*

[1]Department of Electrical and Information Engineering, Politecnico di Bari, 70126 Bari, Italy
[2]Optoelectronics Research Centre, University of Southampton, Southampton SO17 1BJ, U.K.

Abstract: Uniform Fiber Bragg Grating sensors based on Polarization-Maintaining fibers are designed for simultaneous longitudinal strain and temperature measurement of Carbon Fiber Reinforced Polymer laminates. Panda, Bow tie and Pseudo-rectangle optical fiber shape sections are investigated employing three different embedding methods, for each optical fiber. The simulation accurately takes into account that the fibers are embedded in unidirectional Carbon Fiber Reinforced Polymer and covered between two adhesive polyimide films. An exhaustive, accurate and robust investigation of the mechanisms originating Bragg wavelength shift is developed by considering a complete multiphysical model including: the propagation modes and their interaction, the birefringence, the optomechanical and thermal behaviour of both the optical fiber and the embedding composite material. For the first time, the use of polyimide films is proposed to obtain an increase of temperature sensor sensitivity, reducing the stress-transfer, due to thermal expansion, between the composite laminate and the sensing element. The designed Fiber Bragg Grating sensors are compared and their potential application, for simultaneous strain and temperature measurement of Carbon Fiber Reinforced Polymer is discussed.

Index Terms: Modeling, fiber gratings, theory and design, sensors.

1. Introduction

Composite materials offer excellent mechanical properties such as high stiffness, high specific strength and fatigue resistance. In particular, Carbon Fiber Reinforced Polymers (CFRPs) are applied in aircraft and space structures which require strength-to-weight ratios several times larger than steel or aluminum. They absorb in an extraordinary way the energy of mechanical impact, since their matrix structure distributes the energy in the material volume. For this reason, a low velocity/energy impact does not produce perforation but delamination between CFRP layers with no visible surface manifestation [1]. This results in high maintenance and inspection costs because potentially significant damage events could be unnoticed and periodical preventing actions are needed [2]. In fact, CFRP layers can also have hidden voids that are difficult to be detected and

can exhibit failure mechanisms which are generally much more rapid than those occurring in the traditional alloys.

Fiber Bragg Grating (FBG) based optical sensors are very promising in the field of Structural Health Monitoring (SHM). When applied in industrial mechanical equipment or aerospace/aircraft applications they can be essential elements for increasing the safety. Moreover, they can constitute a suitable route to reduce design constrains, e.g., weight, thus increasing fuel efficiency and so bring down CO_2 emission. FBG sensors are very attractive due to their immunity to electromagnetic interference, reduced size, resistance to harsh environments and real time in situ monitoring [3]–[6]. They can be embedded in composite materials in any particular layer or on the surface of CFRP, providing different responses. Generally, optical fibres are not placed on the surface if not jacketed as they could be easily damaged in-service environments [7].

Polyimide coated optical fibers exhibit very attractive mechanical properties. Polyimide is a high-performance polymer, which allows to operate safely in temperatures up to more than 600 K, allowing the optical fibers to survive in high temperature condition, e.g., after thermally cured embedding processes. A critical point when embedding optical fibers is the adhesion between the polyimide coating and the resin. From our tests, embedding polyimide coated optical fibers in composites does not produce critical problems in structural integrity. The adhesion quality depends upon the polymer considered in the matrix and on the diameter of the fibre, as reported in [8]–[11]. For these reasons, polyimide coated optical fibers are an excellent choice for the construction of embedded FBG strain and temperature sensors.

The detection of in-plane and through-thickness strains of composite has been realized by using polarized light in embedded optical fiber sensors and embedded planar optics [8], [12]–[14]. In order to prevent subsurface delamination between ply-layers, it is useful to take into account through-thickness strains. In general, the Bragg wavelength is sensible to the changes of the physical environment around the device, such as strain, stress, temperature, and pressure [15]–[17].

In this paper, a complete model is ad-hoc developed and validated for the design and analysis of Polarization-Maintaining (PM) FBG sensors embedded in CFRPs. Even if fiber gratings are largely employed, there are few literature papers which report similar investigations [18]. The proposed design takes into account the: i) mechanical and thermal behavior of composite material, ii) electromagnetic modal analysis of optical fibers, iii) spectral response of the grating. The investigation method is exhaustive and more precise with respect to those reported in most of the literature, in which n_{eff} or $\Delta\lambda_B$ are estimated without carrying out modal analyses [12], [19], [20]. Moreover, in this paper, for the first time, we propose the use of solid Adhesive Polyimide Films (APFs) with the aim to improve PM fiber temperature sensitivity and to increase the simultaneous discrimination of temperature/strain changes. Polyimide coating was suggested to enhance the robustness and survivability of the embedded optical fibers during composite material manufacturing process [10], [11]. Anti-sticky polyimide films, were investigated to obtain loosely embedded optical fibers in composite materials for strain-free temperature sensing, i.e., for a complete cancellation of stress transfer in all directions, which is the opposite objective with respect that of our paper [21]. Anyway, to avoid the stress effects, aluminum and copper sheets were preferred as more feasible solution [21]. Differently from anti-sticky polyimide films, APFs, which are sticky polyimide films, are commonly used to join together different CFRP laminates [22]. All these applications of polyimide films are completely different with respect to that of this paper, since we propose APFs as buffer regions, i.e., stress absorption layers, in order to obtain through a proper design a suitable reduction of transversal stress-transfer between the laminate and the optical fiber. In this way, the temperature and strain measurement decoupling is affected by less uncertainty. Three kinds of PM optical fibers are investigated, their performances are compared and the most suitable solution for structural monitoring is identified. The simulation proves that the temperature sensitivity of a polyimide coated Bow tie fiber embedded between two APFs, is larger than the sensitivity of the uncoated fiber optic (without APFs) with an increase of 8.9% and 11.2% respectively for the fast and slow axis. The obtained results pave the way to promising applications to prevent cracking in the composite matrix, carbon fiber collapse and delamination between the layers of the laminate.
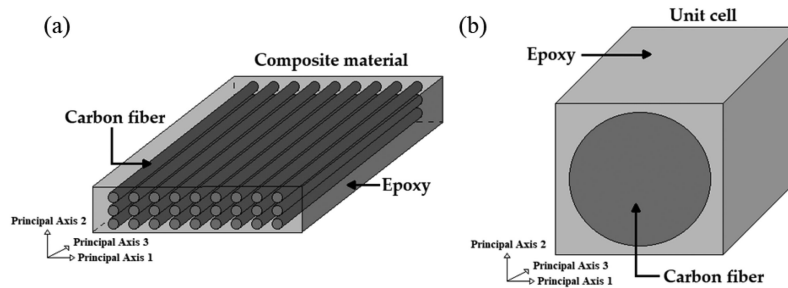
Fig. 1. (a) Schematic representation of CFRP, (b) schematic representation of the unit cell.

The paper is organized as follows: in Section 2, a theoretical introduction about composite materials, PM fibers and sensor operation is illustrated; in Section 3, the strategy pursued for sensor simulation and the validation of the model, the composite material and optical fibers characterization, including the related results of the Finite Element Method (FEM) simulations; in Section 4, a comparison between the sensitivities to strain and temperature of the three optical fibers; in Section 5, our findings and their potential applications are outlined.

2. Recall of Theory on CFRP and Optical Fiber

CFRP is composed of carbon fibers and thermosetting resin. Fig. 1 illustrates a schematic representation of a CFRP (a) and of its unit cell (b). The carbon fibers (dark grey) and thermosetting resin (soft grey), i.e., the two primary components of composite materials, are used to perform a reinforced matrix construction, contributing to CFRP strength. Carbon fibers carry the load, while resin uniformly distributes the load into the material volume. The unit cell is an elementary cubic volume of CFRP including one carbon fiber segment.

The identification of the mechanical properties of each carbon fiber in every layer of the laminate is practically unfeasible. For this reason, it is necessary to estimate the homogenized elasticity matrix to model the average mechanical behavior of a single layer. This is possible by performing a micromechanical analysis on a representative unit cell (Fig. 1).

The elasticity matrix $[\mathbf{C}]_\mathbf{m}$ is evaluated via COMSOL Multiphysics using an inner mathematical model based on solid mechanics theory. In order to introduce the physical quantities relevant for laminate characterization, the Hooke's law, that relates stress and strain is recalled:

$$[\mathbf{e}]_\mathbf{m} = [\mathbf{C}]_\mathbf{m}[\sigma]_\mathbf{m} \tag{1}$$

where $[\mathbf{e}]_\mathbf{m}$ is the strain matrix, $[\mathbf{C}]_\mathbf{m}$ is the elasticity matrix and $[\sigma]_\mathbf{m}$ is the stress matrix. Since the CFRP laminates are constituted by orthotropic material, the elasticity matrix $[\mathbf{C}]_\mathbf{m}$ has all terms nonzero depending on the chosen reference system [23].

High birefringence can be induced in the core of the fibers by two Stress Applying Parts (SAPs). For these fibers a stress-induced birefringence occurs. Other PM fibers exhibit birefringence intrinsically induced by their peculiar geometrical shape, which could be microstructured or simply characterized by axial asymmetry in term of refractive index, without exploitation of stress effects obtained during the fabrication. The SAP consists of a material with a thermal expansion coefficient α different from that of the optical fiber cladding which gives rise to a stress field in the optical fiber. The birefringence induced by the elasto-optic effect depends on the constituent material (e.g., level of dopant concentration), the shape and the positions of the SAPs. This leads to a strong difference in the propagation constant of light travelling through the fiber for the two perpendicular polarizations. In other words, the induced birefringence breaks the circular symmetry of the optical fiber, creating two principal transmission axes within the fiber, known as the fast and slow axes of the fiber.

The coordinate system for optical fiber is the same of that employed for the CFRP illustrated in Fig. 1: the principal axis 1 is parallel to the slow axis, the principal axis 2 to the fast axis and principal axis 3 to the direction of propagation. The refractive index tensor of the optical fiber is diagonal [24]:

$$n_1 = n_0 - C_1 S_{11} - C_2 (S_{22} + S_{33}) \tag{2}$$

$$n_2 = n_0 - C_1 S_{22} - C_2 (S_{33} + S_{11}) \tag{3}$$

$$n_3 = n_0 - C_1 S_{33} - C_2 (S_{11} + S_{22}) \tag{4}$$

Where $\mathbf{S}$ is the internal stress tensor; C_1 and C_2 the stress-optic coefficient and can be evaluated as expressed in (5, 6) [25]:

$$C_1 = \frac{n^3}{2E} (p_{11} - 2\upsilon p_{12}) \tag{5}$$

$$C_2 = \frac{n^3}{2E} (p_{12} - \upsilon (p_{11} + p_{12})) \tag{6}$$

p_{11}, p_{12} are the Pockel's coefficient, n is the refractive index, υ the Poisson's ratio and E the Young's modulus.

The refractive index n changes with external strain $\mathbf{e}$, caused by the tensile stress σ, and temperature variation ΔT [26]:

$$\Delta n_1 = -\frac{n_1^3}{2}(p_{11}e_1 + p_{12}(e_2 + e_3)) + \left(\frac{dn}{dT}\right)\Delta T + \frac{n_1^3}{2}(p_{11} + 2p_{12})\alpha\Delta T \tag{7}$$

$$\Delta n_2 = -\frac{n_2^3}{2}(p_{11}e_2 + p_{12}(e_1 + e_3)) + \left(\frac{dn}{dT}\right)\Delta T + \frac{n_2^3}{2}(p_{11} + 2p_{12})\alpha\Delta T \tag{8}$$

$$\Delta n_3 = -\frac{n_3^3}{2}(p_{11}e_3 + p_{12}(e_1 + e_2)) + \left(\frac{dn}{dT}\right)\Delta T + \frac{n_3^3}{2}(p_{11} + 2p_{12})\alpha\Delta T \tag{9}$$

dn/dT is the thermo-optic coefficient, ΔT the temperature variation, e_1, e_2 (transverse strains) and e_3 (longitudinal strain) are the strain elements of the diagonal tensor, neglecting shear strain.

The thermal expansion coefficient to be used in relations (7–9) is affected by the presence of the composite structure and it is generally smaller than that of the standalone optical fiber. Therefore, there is a great limitation on the term related to thermal expansion, $\alpha\Delta T$, slightly affecting the temperature sensitivity. Temperature changes cause radial strains within the composite material which differ each other. The grating period variation $\Delta\Lambda$ of the grating as a function of the longitudinal strain is described by $\Delta\Lambda = \Lambda e_3$.

The reflection spectra of the Bragg gratings are obtained through the Transfer Matrix Method (TMM) [27]. Each axis in case of PM fibers has a different response to strain Δe_3 and temperature ΔT so that it is possible to solve the following, enabling their discrimination:

$$\begin{pmatrix} \Delta\lambda_{B1} \\ \Delta\lambda_{B2} \end{pmatrix} = \begin{pmatrix} K_{e1} & K_{T1} \\ K_{e2} & K_{T2} \end{pmatrix} \begin{pmatrix} \Delta e_3 \\ \Delta T \end{pmatrix} \tag{10}$$

where subscripts 1, 2 indicate the slow and fast axis, respectively; K_{e1}, K_{e2}, K_{T1}, K_{T2} are the sensitivities to longitudinal strain e_3 and temperature variation ΔT, $\Delta\lambda_{B1}$ and $\Delta\lambda_{B2}$ are the Bragg wavelength shifts.

3. CFRP and Optical Fiber Models

3.1 Simulation Approach

In this paper, a complete model is ad-hoc developed and validated for the design of FBG sensors embedded in CFRP for SHM applications, via COMSOL Multiphysics. The first part of this approach involves the implementation of a 3D-FEM model of a CFRP laminate with the embedded optical
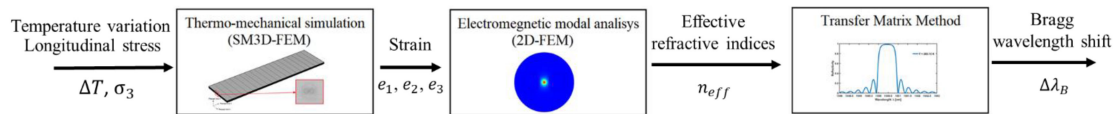
Fig. 2. Flow diagram of the simulation blocks.

fiber under investigation (in the following indicated as SM3D-FEM), to investigate the thermo-mechanical behaviour when external mechanical and thermal stresses are applied. The proposed SM3D-FEM is based on an accurate micromechanical model of the unit cell in order to evaluate the effective elasticity matrix (1). This allows to obtain equivalent homogeneous elasticity matrix of the composite layer. In the SM3D-FEM the fiber optic is 3D-modelled with its mechanical and thermal parameters and it can be embedded in the composite, in every position and orientation. This permits an accurate simulation of the stress-transfer, between the laminate and the optical fiber. In this way, it is possible to simulate strain distribution inside the optical fiber. The strains evaluated along the three principal axes (longitudinal strain e_3 and the two transverse strains e_1, e_2) via thermal and mechanical simulations are used for the successive modal analysis (2D-FEM) of the optical fiber. The fundamental mode HE_{11} is well confined and, by simulation, the presence of the CFRP can be neglected in the 2D-FEM analysis without significant approximation [28]. Considering the small dimensions of an FBG, we can assume that the stress induced by composite material cooling (after curing process) is constant in the FBG region, resulting in the bias of Bragg wavelength λ_B not affecting the sensitivity [29]. Therefore, in our model we neglect this effect originated by fabrication process according to [29]. In particular, the use of the relations (7)-(9) allows to describe the refractive index changes n considering the influence of strain and temperature. The effective refractive indices n_{eff} of the fast and slow propagating modes are found through the 2D-FEM modal analysis. The effective refractive indices n_{eff} are used as input for the home-made software implementing the TMM. This method is considered for the simulation of the reflection spectra of the gratings and the consequent Bragg wavelength shifts $\Delta\lambda_B$, due to the perturbations applied externally to the system. Fig. 2 illustrates the simulation approach with a flux diagram of the main calculation blocks.

Lastly, it is important to underline that the proposed method has intrinsic advantages in terms of accuracy and reliability with respect to other ones reported in literature where n_{eff} or $\Delta\lambda_B$ are estimated without modal analyses [12], [19], [20]. In fact, we model at first the materials and then perform the electromagnetic simulation without approximations.

3.2 Validation of Composite Laminate and FBG Models

In order to validate the SM3D-FEM design approach, experimental data pertaining the tensile mechanical properties of bidirectional carbon fiber composites reinforced in epoxy matrix reported in literature is considered [30]. The considered carbon fiber is Toray T620. The composite laminate, investigated in [30], consists of four layers overlapped, each characterized by a thickness $T_L = 0.75$ mm, a length $L_L = 150$ mm and a width $W_L = 20$ mm. The elasticity matrix $[\mathbf{C}]_\mathbf{m}$ of a composite layer is evaluated through the micromechanical analysis of the unit cell by considering a carbon fiber-resin volume fraction $v_f = 0.563$. The values of Young's Modulus E, Poisson's ratio v, Shear modulus G and density ρ, used for the analysis, are reported in Table 1 [30], [31].

The simulation is in very good agreement with the experiment as shown in Fig. 3, illustrating the tensile stress σ versus e_3 strain simulated via SM3D-FEM (red dash dotted curve); and measured (blue curve) [30]. A little discrepancy can be noted. It is possible to observe that the experimental curve has an almost linear trend up to a strain value close to $e_3 = 1.7\%$. In the actual behaviour, after the abovementioned value the rupture point of the material is observed.

TABLE 1

Mechanical and Thermal Properties of Composite Carbon Fiber and Epoxy Resin

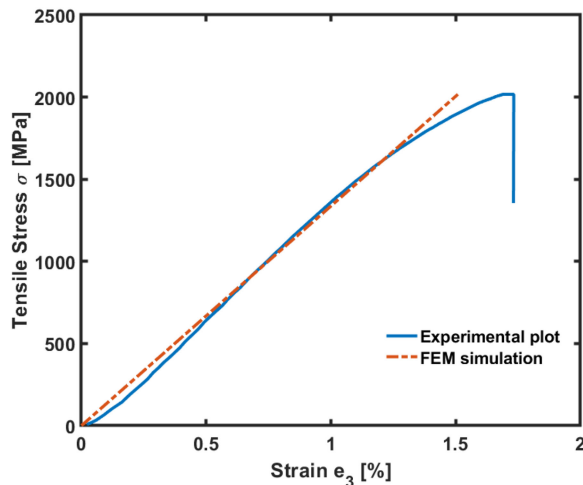| Parameter	Symbol	Value carbon fiber	Value epoxy	Unit
Young's modulus	E	235 (33 direction)	3.1	GPa
		15 (11 direction)		
Shear modulus	G	50 (31 direction)	-	GPa
		50 (12 direction)		
Poisson's ratio	v	0.23 (31 direction)	0.35	-
		0.23 (12 direction)		
Density	ρ	1770	1130	kg/m^3

Fig. 3. Tensile stress σ versus e_3 strain. Simulation via SM3D-FEM solver (red curve); experiment (blue curve) reported in [30].

In the simulation of the stress-strain curve only the elastic behaviour is evaluated because in unidirectional composite laminates there is no plastic deformation and consequently, they have an almost elastic behaviour [31], [32].

The developed home-made computer code based on TMM has been validated giving optimum agreement with literature results [3], [17], [27].

3.3 Opto-mechanical Simulation

Three different kinds of PM optical fibers are taken into account, whose geometric and physical parameters employed for the simulation are taken from literature papers [24], [33]–[35]. We investigated Panda, Bow tie and Pseudo-rectangle optical fibers considering three different embedding techniques: i) embedding in CFRP without coating, without APFs, Fig. 4(a); ii) embedding in CFRP with polyimide coating, without APFs, Fig. 4(b); iii) embedding in CFRP with polyimide coating and covered between two APFs, Fig. 4(c) and (d). Therefore, a total of nine cases are investigated.

The optomechanical and electromagnetic investigation exactly takes into account the geometries and physical properties of the abovementioned nine sensors embedded in the CFRP. Fig. 4 refers only to the case of Panda fiber, to avoid useless repetitions.

The cladding for all the considered optical fibers is made of pure Silica, the core is doped with GeO_2 while the SAPs are doped with B_2O_3. The physical parameters employed in the simulation are reported in Table 2 and are taken from literature [26]. In the case of the Pseudo-rectangle fiber, the inner cladding is fluorine doped [33], and has refractive index $n_{icl} = 1.4404$, while the thermal
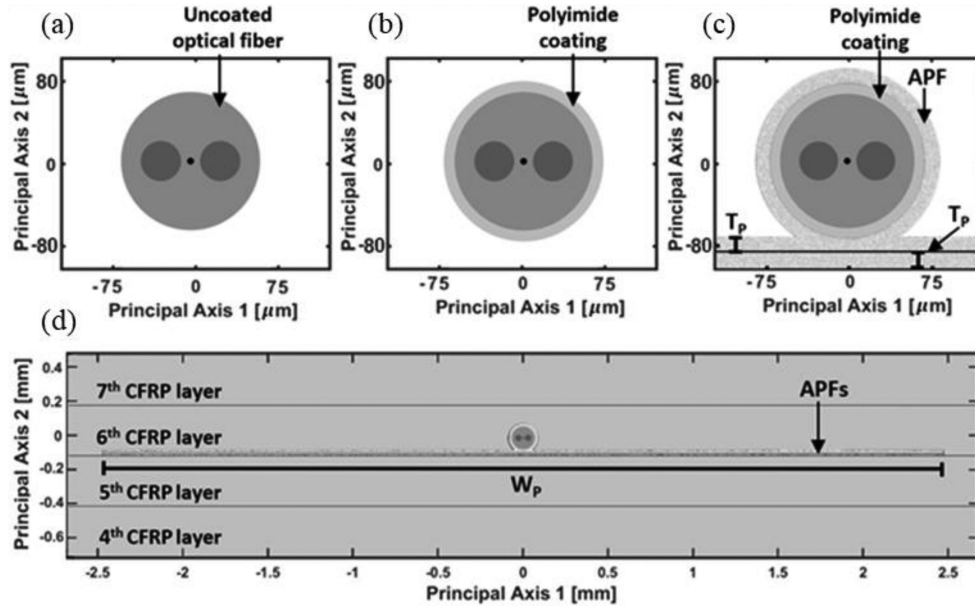
Fig. 4. Cross-section of Panda fiber: (a) without coating, (b) with polyimide coating, (c) with polyimide coating and covered between two APFs, (d) with polyimide coating, covered between two APFs and embedded in the CFRP laminate, $T_p = 0.03$ mmand $W_p = 5$ mm.

TABLE 2

Common Parameters of the Simulated Optical Fibers

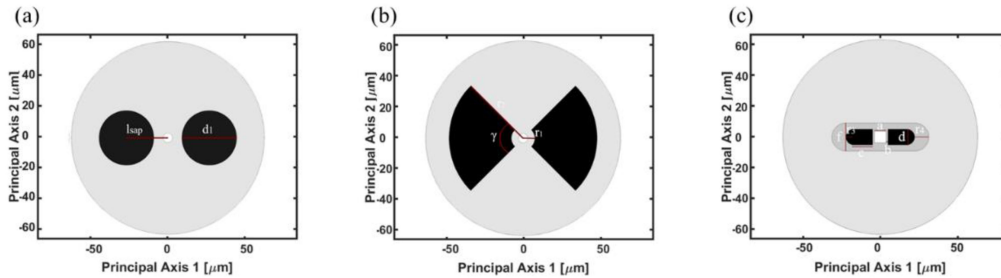| Parameter	Symbol	Core	Cladding	SAP	Unit
Refractive index	n	1.448	1.444	1.4384	-
Young's modulus	E	70.7	73.9	50	GPa
Poisson's ratio	v	0.1708	0.170	0.200	-
Thermal expansion coefficient	α	7.08×10^{-7}	5.6×10^{-7}	20×10^{-7}	$1/K$

Fig. 5. Cross-sections of the investigated PM fibers: (a) Panda, (b) Bow tie, (c) Pseudo-rectangle.

expansion coefficient is $\alpha_{icl} = 5.0 \times 10^{-7} 1/K$. For all the optical fibers, the stress-optical coefficients are $C_1 = 0.757 \times 10^{-12} \ m^2/N$ and $C_2 = 4.188 \times 10^{-12} \ m^2/N$. The thermo-optic coefficient is $dn/dT = 9.15 \times 10^{-6} \ K^{-1}$, the Pockel's coefficients are $p_{11} = 0.121$ and $p_{12} = 0.27$ [34].

For all the three fibers the cladding diameter is $d_{cl} = 125 \ \mu$m. For the Panda fiber, the distance between the centres of the core and of the SAP is $l_{SAP} = 26.8 \ \mu$m, SAP has a diameter $d_1 = 35.5 \ \mu$m (see Fig. 5(a)) [35]. For the Bow tie fiber, the position of the SAP is given by $r_1 = 7.5 \ \mu$m, $r_2 = 47.5 \ \mu$m, $\gamma = 90°$ (see Fig. 5(b)) [24]. These two fibers have a circular core

TABLE 3

Mechanical and Thermal Properties of Carbon Fiber, Epoxy Resin and Polyimide

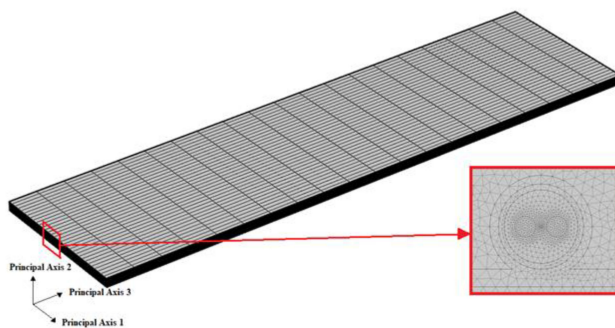| Parameter	Symbol	Value carbon fiber	Value epoxy	Value polyimide	Unit
Young's modulus	E	230 (33 direction) 15 (11 direction)	4	3.1	GPa
Shear modulus	G	24 (31 direction) 5.03 (12 direction)	-	-	GPa
Poisson's ratio	v	0.2 (31 direction) 0.07 (12 direction)	0.35	0.35	-
Thermal expansion coefficient	α	-0.6×10^{-6} (// fiber direction) 8.5×10^{-6} ($\perp$ fiber direction)	55×10^{-6}	60×10^{-6}	$1/K$
Density	ρ	1800	1100	1300	kg/m^3

Fig. 6. Mesh of the CFRP laminate and zoom of the mesh cross-section in correspondence of the PM optical fiber.

with diameter $d_{co} = 6 \ \mu$m. The Pseudo-rectangle fiber has a square core of side $a = 7.5 \ \mu$m. $b = 1.25 \ \mu$m, $c = 12 \ \mu$m, $d = 10 \ \mu$m, $f = 18 \ \mu$m, $r_3 = 5 \ \mu$m, $r_4 = 9 \ \mu$m (see Fig. 5(c)) [33].

The mechanical and thermal properties of the composite material used for the modelling of CFRP laminates are described in [32], [36], while the specimen sizes agree with those typically used to perform structural tests.

The carbon fiber-resin volume fraction is $v_f = 0.6$ and the values of Young's Modulus E, Poisson's ratio v, Shear modulus G and density ρ listed in Table 3 [36], [37]. The layer thermal expansion coefficient in the carbon fiber direction (principal axis 3) $\alpha_{//} = 3.7249 \cdot 10^{-8}$ and perpendicular to carbon fiber direction (principal axes 1 and 2) $\alpha_\perp = 3.4718 \cdot 10^{-5}$ are evaluated considering the layer Poisson's ratio $v_{31} = 0.26$. The unidirectional composite laminate has eight layers, each characterized by a thickness $T_L = 0.3 \ mm$, length $L_L = 150 \ mm$ of and a width $W_L = 40 \ mm$.

In all cases, the optical fiber sensor is placed on the sixth layer of the CFRP laminate. Apart from the case of uncoated optical fiber, the polyimide coating has a diameter of $d_{coat} = 145 \ \mu$m. In the case iii), the fiber optic is covered between two APFs, see Fig. 4(c) and 4(d). The thickness T_P and the width W_P of both the APFs have been optimized as successively described. The same cases shown in Fig. 4 for Panda fiber are also investigated for the Bow tie and Pseudo-rectangle optical fibers, i.e., nine different optical sensors are investigated. The mechanical and thermal parameters of carbon fiber, epoxy resin and polyimide are described in Table 3. The number of mesh elements is close to $N_E = 317900$ (Fig. 6).

For the stress analysis, a range of tensile stress from $\sigma = 0$ MPa to $\sigma = 60$ MPa along the principal axis 3 (Fig. 1) with a step of 10 MPa is considered; for thermal analysis, a range of temperature from $T = 233.15$ K to $T = 368.15$ K with a step of 15 K. Fig. 7(a) refers to the
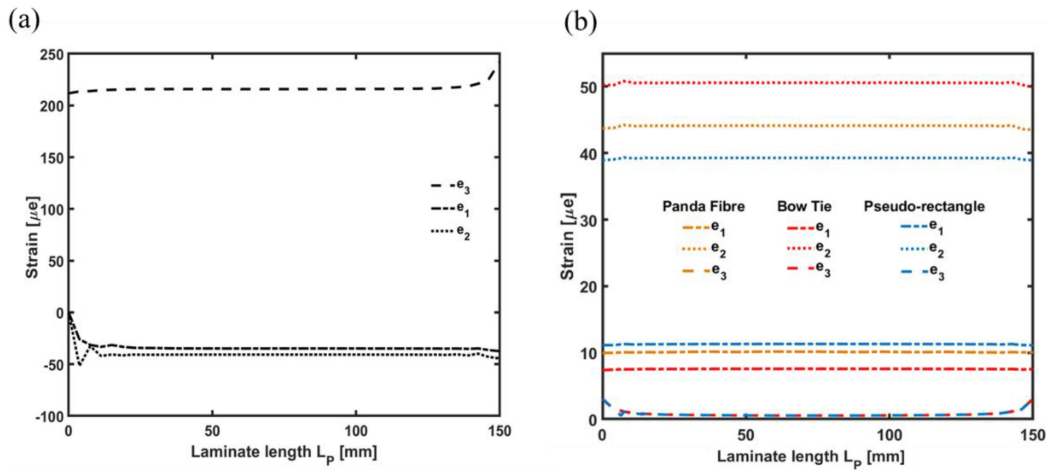
Fig. 7. (a) Strain distribution inside the polyimide coated PM optical fibers, covered between two APFs and embedded in CFRP, versus the laminate length: tensile stress $\sigma = 30$ MPa without temperature variation. (b) Strain distribution inside the polyimide coated PM optical fibers, covered between two APFs and embedded in CFRP, versus the laminate length: temperature $T = 308.15$ K is reached without applying stress.

case of polyimide coated PM fiber, covered between two APFs and embedded in CFRP subjected to tensile stress σ.

Fig. 7(a) depicts the strain distribution versus the laminate length L_P along the principal axes, evaluated at the center of the optical fiber core for the reference temperature $T_{ref} = 293.15$ K when a tensile stress $\sigma = 30$ MPa is applied. The longitudinal strain e_3 (dashed curve) is related the transverse strains e_1 (dash dotted curve) and e_2 (dotted curve) through the Poisson's ratio. The strain distributions of Fig. 7(a) can be practically considered identical for Panda, Bow tie and Pseudo-rectangle fibers since the optical fibers, with same cladding diameter and coating, influence the response of the CFRP laminate to tensile stress σ in a similar way and very slightly. In Fig. 7(a), as expected, the laminate ends exhibit strain changes/oscillations because of the constraint reaction. The mesh shown in Fig. 6 is coarse in the direction of principal axis 3, thus we cannot conclude with confidence about the strain values at the laminate edges. However, these values are not of our interest since the FBG sensor has small length and placed where the strains are constant, far from the edges. Fig. 7(b) shows the strains at temperature $T = 308.15$ K without applying stress $\sigma = 0$ MPa, for the case of polyimide coated PM fibers, covered between two APFs and embedded in CFRP. Moreover, Fig. 7(b) illustrates the strain distribution for the three considered PM fibers. The longitudinal strain e_3 (dashed curve) is close to 0 μe, so that the length of the laminate L_L does not change significantly.

In the 2D-FEM optical mode investigation, the variation of the refractive indices n with respect to the internal stress tensor S is simulated taking into account the thermal expansion coefficient α, Young's Modulus E, Poisson's ratio v according to eq. (2)–(4). The propagating modes are calculated at the wavelength $\lambda = 1550$ nm. The fictive temperature $T_{fict} = 1273.15$ K, at which the glass begins to behave elastically and the reference temperature $T_{ref} = 293.15$ K, in unperturbed condition, both affecting the internal thermal stress, are considered. Birefringence B depends on the difference between the fictive temperature T_{fict} and the operation temperature T, the former pertaining to the fabrication process the latter to the operation condition [24], [38], [39].

The two different polarizations of the fundamental mode propagate at different velocities. The effective refractive indices n_{eff}, in absence of external strain fields e and temperature variation ΔT, highlights a higher degree of birefringence B for the Bow tie fiber. Fig. 8 shows the simulated internal stress distributions S_{11} in the Panda, Bow tie and Pseudo-rectangle fibers cross-section
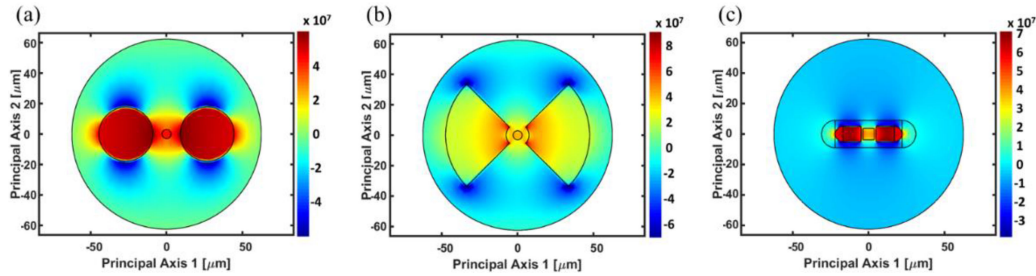
Fig. 8. Simulated internal stress distribution S_{11} [N/m^2] in unperturbed condition: (a) Panda, (b) Bow tie, (c) Pseudo-rectangle.
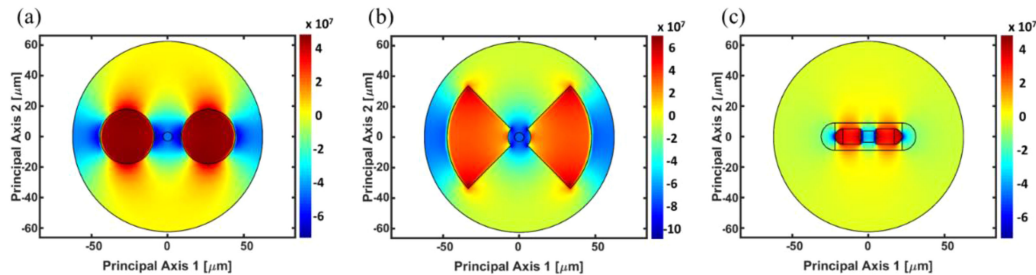

Fig. 9. Simulated internal stress distribution S_{22} [N/m^2] in unperturbed condition: (a) Panda, (b) Bow tie, (c) Pseudo-rectangle.
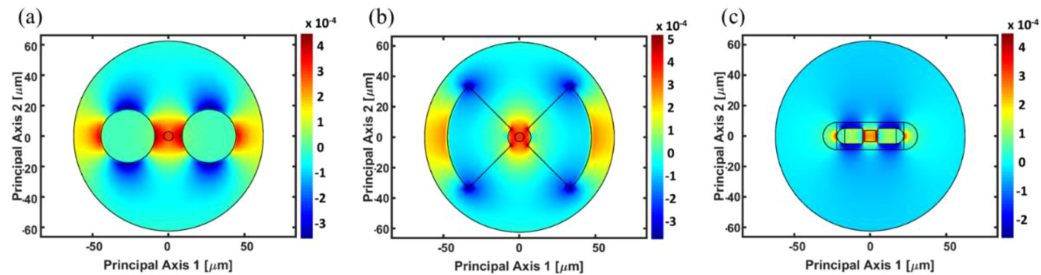

Fig. 10. $n_1 - n_2$ in the optical fiber cross-section in unperturbed condition: (a) Panda, (b) Bow tie, (c) Pseudo-rectangle.

in unperturbed condition (in absence of temperature variation ΔT and tensile stress σ). For all the three kinds of optical fibers considered in Fig. 8, the SAPs are subjected to a compressive stress (red colour), this means that these regions are shrinking. This happens since the thermal expansion coefficient α of the SAPs is higher than the surrounding cladding. With the exception of the region of the core, that is mainly compressed (red colour), it is also possible to see that the SAPs pull apart and compress, along the principal axis 1, the immediate cladding area around them. Along the principal axis 2, towards the SAPs, the neighboring cladding area is expanded (blue colour). Toward the outer edge of the cladding, the stress intensity tends to $S_{11} = 0$ N/m^2, signifying that this region is not strongly compressed or under tension. In Fig. 9, it is possible to observe that, also in this case, the SAPs region is shrinking but the compression is distributed along the principal axis 2 near the SAPs. Birefringence B is proportional to the difference in stress distributions S_{11} and S_{22} [24]. Considering Fig. 10, it is evident that Bow tie fiber shows a higher degree of Birefringence B, since the difference between n_1 and n_2 is larger. The SAPs of the pseudo

TABLE 4

Parameters of the Simulated Uniform FBG for Both Panda, Bow Tie and Pseudo-rectangle Fibers

Parameter	Symbol	Value	Unit
Grating Period	Λ	0.5365	μm
Amplitude of index modulation	m	7×10^{-4}	-
FBG length	L	2000	μm

TABLE 5

Sensitivity to Temperature Variation ΔT of the Simulated FBG Written in PM Fibers, Considering the Optical Fiber Without Coating and with Polyimide Coating

Parameter	Symbol	Uncoated	Polyimide coating	Unit
Panda sensitivity to temperature – slow axis	K_{t1}	7.259	7.952	pm/K
Panda sensitivity to temperature – fast axis	K_{t2}	8.647	9.127	pm/K
Bow tie sensitivity to temperature – slow axis	K_{t1}	7.237	7.681	pm/K
Bow tie sensitivity to temperature – fast axis	K_{t1}	8.720	9.135	pm/K
Pseudo-rectangle sensitivity to temperature – slow axis	K_{t1}	7.579	8.219	pm/K
Pseudo-rectangle sensitivity to temperature – fast axis	K_{t1}	8.752	9.180	pm/K

rectangle are geometrically smaller than the ones of Panda and Bow tie fiber and thus slightly affect the Poisson's ratios v along the slow axis. This leads to very close slow and fast strain sensitivities if compared with the other two investigated PM optical fibers. This evidences how the design of ad-hoc fiber cross-section, the use of specific dopants and their concentrations allow to hand the stress birefringence.

Fig. 10 shows the difference between n_1 and n_2 in unperturbed condition for the considered PM fibers: the stress anisotropy leads to refractive index anisotropy through the stress-optical coefficients [40].

4. Performance Comparison of FBGs Embedded in CFRP Laminate

The three PM fibers of Figs. 8–10, Panda, Bow tie, Pseudo-rectangle, are investigated and compared in the cases of Fig. 4: i) without coating, ii) with polyimide coating, iii) with polyimide coating and APFs. The nominal parameters of the gratings, i.e., without/before applying external perturbations and at the reference temperature T_{ref} are reported in Table 4. The amplitude of index modulation m and the length of the grating L ensure good coupling and high reflectivity.

Table 5 reports the sensitivities simulated in the case of uncoated and polyimide coated for all the three PM fibers. Moreover, only the temperature sensitivities are reported since the polyimide does not affect strain sensitivity. It can be noticed that its introduction improves the performance of the sensor.

The thickness T_P and the width W_P of the two APFs have been optimized via a parametric investigation. The width W_P has been varied from 1 mm to 9 mm with a step of 2 mm. The temperature sensitivity remains almost unchanged by changing the width W_P. Therefore, $W_P = $ 5 mm has been chosen because it being a feasible value for an easy implementation and for preventing undesirable crack. Also, the thickness T_P has been optimized. The investigation results regarding the Bow tie fiber are listed in Table 6. It is evident that by increasing thickness T_P , the sensitivity becomes greater. The drawback is that a too large thickness T_P, could lead to a decreasing of composite material mechanical robustness. We selected $T_P = $ 0.03 mm, since it is a good trade-off between sensitivity and probability of failure within the CFRP laminate. The longitudinal strain sensitivity is not affected by variation in APFs size.

TABLE 6

Sensitivity to Temperature ΔT and Thickness T_P Variation of the Simulated FBG Written in Polyimide Coated Bow Tie Fiber, Covered Between Two APFs and Embedded in CFRP (polyimide Width Is Considered Constant and Equal to $W_P = 5$ mm)

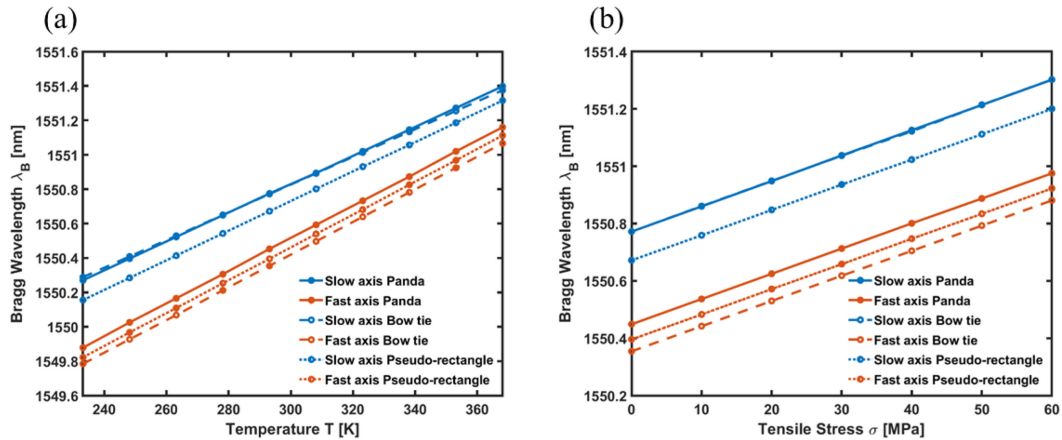| Parameter	Symbol	Value					Unit
Polyimide film thickness	T_P	0.01	0.02	0.03	0.04	0.05	mm
Sensitivity to temperature – slow axis	K_{t1}	7.830	7.950	8.051	8.097	8.160	pm/K
Sensitivity to temperature – fast axis	K_{t2}	9.284	9.402	9.497	9.550	9.608	pm/K

Fig. 11. (a) Bragg wavelength λ_B versus the temperature T simulated for both slow (blue colour) and fast (red colour) axes; Panda (continuous line), Bow tie (dashed line), Pseudo-rectangle (dotted line) coated with polyimide, covered between two APFs and embedded in CFRP. Grating parameter: $\Lambda = 0.5365~\mu m$, $m = 7 \times 10^{-4}$, $L = 2000~\mu m$. (b) Bragg wavelength λ_B versus the tensile stress σ simulated for both slow (blue colour) and fast (red colour) axes; Panda (continuous line), Bow tie (dashed line), Pseudo-rectangle (dotted line) coated with polyimide, covered between two APFs and embedded in CFRP. Grating characteristics: $\Lambda = 0.5365~\mu m$, $m = 7 \times 10^{-4}$, $L = 2000~\mu m$.

From this point on, the investigation is focused on the case of the optical fibers coated with polyimide, covered between two APFs and embedded in CFRP. The two APFs have dimensions $T_P = 0.03$ mm and $W_P = 5$ mm. The three PM fibers exhibit a linear response of the Bragg wavelength λ_B versus the temperature T as evident in Fig. 11(a) for both slow (blue colour) and fast (red colour) axes of Panda (continuous line), Bow tie (dashed line), Pseudo-rectangle (dotted line) optical fibers.

In Fig. 11(a) it is possible to observe that Panda (continuous line) and Bow tie (dashed line) have similar Bragg wavelength in the nominal condition ($T_{ref} = 293.15$ K) for the slow axis: the characteristics are almost coincident. Similar considerations can be made for Fig. 11(b), depicting the Bragg wavelength shift $\Delta\lambda_B$ versus the tensile stress σ simulated for both slow (blue colour) and fast (red colour) axes. Table 7 shows the calculated sensitivity for each axis of each PM fiber analysed. The obtained results highlight that the Bow tie optical fiber shows better performances in terms of decoupling strain and temperature changes, achieving temperature sensitivities of 8.051 pm/K and 9.497 pm/K and strain sensitivities of 1.229 $pm/\mu e$ and 1.220 $pm/\mu e$, for the slow and the fast axis respectively. The sensitivity matrix determinant is the highest and thus the system (10) is better-conditioned. Furthermore, by using the relation (10), it is possible to calculate simultaneously the strain Δe_3 and temperature ΔT changes with a single optical fiber. By comparing uncoated fiber without APFs and polyimide coated fiber with APFs an increase of temperature sensitivity for the Bow tie optical fiber fast and slow axis roughly of 8.9% and 11.2% respectively is obtained, as reported in Table 5 and Table 7. According to [41], uncertainties on

TABLE 7

Sensitivity to Temperature Variation $\triangle T$ and Longitudinal Strain e_3 of the Simulated FBG Written in Polyimide Coated PM Fibers, Covered Between Two APFs and Embedded in CFRP

Parameter	Symbol	Panda	Bow tie	Pseudo-rectangle	Unit
Sensitivity to strain – slow axis	K_{e1}	1.229	1.229	1.224	$pm/\mu e$
Sensitivity to strain – fast axis	K_{e2}	1.222	1.220	1.220	$pm/\mu e$
Sensitivity to temperature – slow axis	K_{t1}	8.356	8.051	8.596	pm/K
Sensitivity to temperature – fast axis	K_{t2}	9.499	9.497	9.557	pm/K

TABLE 8

Uncertainty to Temperature Variation δT and Longitudinal Strain δe_3 of the Simulated FBG Written in Polyimide Coated PM Fibers, Covered Between Two APFs and Embedded in CFRP for an Interrogator Resolution of $\delta \lambda_B = 1 \; pm$

Parameter	Temperature	Strain
	Uncertainty $\boldsymbol{\delta T}$ $[K]$	Uncertainty $\boldsymbol{\delta e_3}$ $[\mu e]$
Panda with coating and APFs	1.68	12.20
Bow tie with coating and APFs	1.32	9.49
Pseudo-rectangle with coating and APFs	2.02	14.99

strain and temperature can be computed knowing the interrogator wavelength resolution $\delta\lambda_B$ and sensitivity matrix K_S (10). Uncertainty to temperature variation δT and longitudinal strain δe_3 of the simulated FBG written in polyimide coated PM fibers, covered between two APFs and embedded in CFRP is reported in Table 8 for an interrogator with wavelength resolution of $\delta \lambda_B = 1 \; pm$. It is evident by analysing the uncertainties values reported in Table 8 that the Bow tie fiber is the most suitable for the decoupling. The effect of the polyimide coating and APFs lead to similar percentage increase of temperature sensitivities for all the three simulated optical fibers. Moreover, APFs make simpler the manufacturing process of the composite material, simplifying the alignment of fast and slow axis of PM optical fibers in CFRP layers. They can be easily fabricated by placing liquid polyimide solution onto the fiber and then putting this on a solid polyimide film. Basically, the fabrication process consists of two phases, a soft-bake process considering a temperature $T \cong 410 \; K$ and a time of curing $t \cong 10'$ followed by a hard-bake process ($T \cong 520 \; K$, $t \cong 30'$). As an alternative a spin-coating technique can be employed.

5. Conclusion

In this paper, a comprehensive approach has been developed for the accurate study of three PM fibers (Panda, Bow tie and Pseudo-rectangle) embedded in CFRP. The design of two APFs, covering the fiber optic sensors, is proposed. Numerical results suggest that by adding suitable APFs embedding the polyimide coated optical fibers it is possible to perform a more accurate strain and temperature measurement with respect to uncoated or conventional polyimide coated optical fibers (without APFs). In particular, the temperature sensitivity for both slow and fast axis can be increased of about 10% for all the investigated optical fibers. By comparing the simulation results obtained for the PM optical fibers polyimide coated and covered between APFs, the Bow tie optical fiber shows the lowest values of uncertainty to temperature variation $\delta T = 1.32 \; K$ and to longitudinal strain $\delta e_3 = 9.49 \; \mu e$. We can conclude that, among the other PM fibers, Bow tie allows the best decoupling of the simultaneous temperature and strain measurement. Moreover, the introduction of APFs improve the manufacturing process of composite material, simplifying the alignment of fast and slow axis of PM optical fibers in CFRP layers. The next step will be the experimental investigation of the simulated results with the construction of the sensor prototypes.

Acknowledgment

References

[1] C. Bonavolontà, M. Valentino, G. Peluso, and A. Barone, "Non destructive evaluation of advanced composite materials for aerospace application using HTS SQUIDs," *IEEE Trans. Appl. Supercond.*, vol. 17, no. 2, pp. 772–775, Jun. 2007.

[2] G. Williams, R. Trask, and I. Bond, "A self-healing carbon fibre reinforced polymer for aerospace applications," *Composites Part A: Appl. Sci. Manuf.*, vol. 38, no. 6, pp. 1525–1532, 2007.

[3] W. Scarcia, G. Palma, M. C. Falconi, F. De Leonardis, V. M. N. Passaro, and F. Prudenzano, "Electromagnetic modelling of fiber sensors for low-cost and high sensitivity temperature monitoring," *Sensors*, vol. 15, no. 12, pp. 29855–29870, 2015.

[4] M. Sabaeien, H. Nadgaran, M. De Sario, L. Mescia, and F. Prudenzano, "Thermal effects on double clad octagonal Yb:Glass fiber laser," *Opt. Mater.*, vol. 31, no. 9, pp. 1300–1305, 2009.

[5] L. Mescia and F. Prudenzano, "Advances on optical fiber sensors," *Fibers*, vol. 2, no. 1, pp. 1–23, 2013.

[6] A. D'Orazio, M. De Sario, C. Giasi, L. Mescia, V. Petruzzelli, and F. Prudenzano, "Design of planar optic sensors for hydrocarbon detection," *Opt. Quantum Electron.*, vol. 36, no. 6, pp. 507–526, 2004.

[7] K. Shivakumar and L. Emmanwori, "Mechanics of failure of composite laminates with an embedded fiber optic sensor" *J. Compos. Mater.*, vol. 38, pp. 669–679, 2004.

[8] C. Holmes, M. Godfrey, D. J. Bull, and J. Dulieu-Bartonc, "Real-time through-thickness and in-plane strain measurement in carbon fiber reinforced polymer composites using planar optical bragg gratings," *Opt. Lasers Eng.*, vol. 133, 2020, Art. no. 106111.

[9] S. Takeda, Y. Okabe, and N. Takeda, "Delamination detection in CFRP laminates with embedded small-diameter fiber bragg grating sensors" *Composites Part A: Appl. Sci. Manuf.*, vol. 33, pp. 971–980, 2002.

[10] C. DiFrancia, R. Claus, J. W. Hellgeth, and T. C. Ward, "Structure/Property correlations of several polyimide optical fiber coatings for embedding in an epoxy matrix," in *Proc. SPIE Fiber Optic Smart Struct. Skins Conf. II*, 1989, vol. 1170, pp. 505–512.

[11] D. K. Nath *et al.*, "Polyimide coated embedded optical fiber sensors," in *Proc. SPIE Structures Sens. Control*, vol. 1489, pp. 17–32, 1991.

[12] X. Zhang *et al.*, "Monitoring the failure forms of a composite laminate system by using panda polarization maintaining fiber bragg gratings," *Opt. Exp.*, vol. 27, no. 13, pp. 17571–17580, 2019.

[13] M. Rosenberger, W. Eisenbeil, B. Schmauss, and R. Hellmann, "Simultaneous 2D strain sensing using polymer planar bragg gratings," *Sensors*, vol. 15, no. 2, pp. 4264–4272, 2015.

[14] J. Missinne *et al.*, "Thin and flexible polymer photonic sensor foils for monitoring composite structures," *Adv. Eng. Mater.*, vol. 20, no. 2, 2018, Art. no. 1701127.

[15] F. Chiavaioli *et al.*, "Long period grating-based fiber coupling to WGM microresonators," *Micromachines*, vol. 9, no. 7, pp. 366–378, 2018.

[16] F. Prudenzano, L. Mescia, T. Palmisano, M. Surico, M. De Sario, and G. C. Righini, "Optimization of pump absorption in MOF lasers via multi-long-period gratings: Design strategies," *Appl. Opt.*, vol. 51, no. 9, pp. 1420–1430, 2012.

[17] L. Mescia, T. Palmisano, M. Surico, and F. Prudenzano, "Long-period gratings for the optimization of cladding-pumped microstructured optical fiber laser," *Opt. Mater.*, vol. 33, no. 2, pp. 236–240, 2010.

[18] T. O. S. Yashiro, N. Toyama, and N. Takeda, "Monitoring damage in holed CFRP laminates using embedded chirped FBG sensors," *Int. J. Solids Struct.*, vol. 44, no. 2, pp. 603–613, 2007.

[19] P. G. F.Bosia, J. Botsis, M. Facchini, H. G. Limberger, and R. P. Salathé, "Characterization of the response of fibre bragg grating sensors subjected to a two-dimensional strain field," *Smart Mater. Struct.*, vol. 12, no. 6, pp. 925–934, 2003.

[20] X. Geng *et al.*, "Sensing characteristics of FBG sensor embedded in CFRP laminate," *Measurement*, vol. 98, pp. 199–204, 2017.

[21] P. Zhu, J. Wu, M. Huang, Y. Wang, P. Liu, and M. A. Soto, "Reducing residual strain in fiber Bragg grating temperature sensors embedded in carbon fiber reinforced polymers," *J. Light.Technol.*, vol. 37, no. 18, pp. 4650–4656, 2019.

[22] N. Grundmann, H. Brüning, K. Tserpes, T. Strohbach, and B. Mayer, "Influence of embedding fiber optical sensors in CFRP film adhesive joints on bond strength," *Sensors*, vol. 20, no. 26, 2020, Art. no. 1665.

[23] A. Öchsner and M. Öchsner, *The Finite Element Analysis Program MSC Marc/Mentat*. Singapore: Springer, 2016.

[24] R. Guan, F. Zhu, Z. Gan, D. Huang, and S. Liu, "Stress birefringence analysis of polarization maintaining optical fibers," *Opt. Fiber Technol.*, vol. 11, no. 3, pp. 240–254, 2005.

[25] D. J. Lockwood and L. Pavesi, *Silicon Photonics II Components and Integration*. Berlin, Heidelberg, Germany: Springer, 2011.

[26] H. Alemohammad, *Opto-mechanical Fiber Optic Sensors: Research, Technology, and Applications in Mechanical Sensing*, Amsterdam, The Netherlands: Butterworth-Heinemann, 2018.

[27] T. Erdogan, "Fiber grating spectra," *J. Light. Technol.*, vol. 15, no. 8, pp. 1277–1294, 1997.

[28] W. Hu, C. Li, S. Cheng, F. Mumtaz, C. Du, and M. Yang, "Etched multicore fiber Bragg gratings for refractive index sensing with temperature in-line compensation," *OSA Continuum.*, vol. 3, no. 4, pp. 1058–1067, 2020.

[29] G. Rajan, R. Raju, S. Jinachandran, P. Farrar, J. Xi, and B. G. Prusty, "Polymerisation shrinkage profiling of dental composites using optical fibre sensing and their correlation with degree of conversion and curing rate," *Sci. Rep.*, vol. 9, no. 1, 2019, Art. no. 3162.

[30] M. H. Ikbal, "Tensile properties of bidirectional glass-carbon hybrid composites: Part I," [Online]. Available: https://textilefocus.com/tensile-properties-bidirectional-glass-carbon-hybrid-composites-part/

[31] F. Groh, E. Kappel, C. Huhne, and F. Meyer, "Process-induced distortions of composite structures due to through-thickness fibre volume fraction gradients," in *Proc. Eur. Conf. Composite Mater.*, 2016, pp. 26–30.

[32] Z. Zhai, B. Jiang, and D. Drummer, "Tensile creep behavior of quasi-unidirectional E-Glass fabric reinforced polypropylene composite," *Polymers*, vol. 10, no. 6, pp. 661, 2018.

[33] F. Ren *et al.*, "Design of 20-polarization-maintaining-mode 'pseudo-rectangle' elliptical-core fiber for MIMO-less MDM networks," *Opt. Fiber Technol.*, vol. 50, pp. 87–94, 2019.

[34] Z. Han, N. Zhao, Z. Yang, and G. Li, "Error analyses for simultaneous measurement of temperature and strain based on polarization maintaining few-mode fibers," in *Proc. IEEE Asia Commun. Photon. Conf.*, 2018, pp. 1–3.

[35] A. Annunziato *et al.*, "Structural health monitoring of composite laminae for aerospace applications via embedded panda fiber bragg grating," in *Proc. IEEE 22nd Int. Conf. Transparent Opt. Netw.*, 2020, pp. 1–5.

[36] C. Zhang, W. K. Binienda, R. K. Goldberg, and L. W. Kohlman, "Meso-scale failure modeling of single layer triaxial braided composite using finite element method," *Composites Part A: Appl. Sci. Manuf.*, vol. 58, pp. 36–46, 2014.

[37] Z. Zhao, H. Dang, C. Zhang, G. J. Yun, and Y. Li, "A multi-scale modeling framework for impact damage simulation of triaxially braided composites," *Composites Part A: Appl. Sci. Manuf.*, vol. 110, pp. 113–125, 2018.

[38] M. P. Varnham, D. N. Payne, A. J. Barlow, and R. D. Birch, "Analytic solution for the birefringence produced by thermal stress in polarization-maintaining optical fibers," *J. Light. Technol.*, vol. 1, no. 2, pp. 332–339, 1983.

[39] Y. H. Kim, H. Kwon, J. Kim, and K. Y. Song, "Distributed measurement of hydrostatic pressure based on brillouin dynamic grating in polarization maintaining fibers," *Opt. Exp.*, vol. 24, no. 19, pp. 21399–21406, 2016.

[40] J. L. Santos and F. Farahi, *Handbook of Optical Sensors*. CRC Press, 2018.

[41] D. Kinet, P. Mégret, K. W. Goossen, L. Qiu, D. Heider, and C. Caucheteur, "Fiber Bragg grating sensors toward structural health monitoring in composite materials: Challenges and solutions," *Sensors*, vol. 14, no. 4, pp. 7394–7419, 2014.